Magnetic properties of the dense Kondo compound CeSe studied by neutron scattering

1993 J. Phys.: Condens. Matter 5 1119

(http://iopscience.iop.org/0953-8984/5/8/013)

J. Phys.: Condens. Matter 5 (1993) 1119–1132. Printed in the UK

Magnetic properties of the dense Kondo compound CeSe studied by neutron scattering

A Dönni†‡, A Furrer†, P Fischer†, S M Hayden§||, F Hulliger¶ and T Suzuki‡

† Laboratory for Neutron Scattering, ETH Zürich, CH-5232 Villigen PSI, Switzerland
‡ Department of Physics, Faculty of Science, Tohoku University, Sendai 980, Japan
§ Institute Laue–Langevin, F-38042 Grenoble Cédex, France
¶ Laboratory for Solid State Physics, ETH Zürich, CH-8093 Zürich, Switzerland

Received 11 November 1992

Abstract. Magnetic properties of the FCC type II antiferromagnetic CeSe have been studied by elastic, diffuse critical and inelastic neutron scattering experiments. The diffuse critical scattering above the Néel temperature corresponds to highly anisotropic longitudinal spin fluctuations with a lenslike intensity distribution. The magnetic phase diagram for fields along the $[1\bar{1}0]$ direction contains a first-order magnetic phase transition at $H = H_{crit}(T) \leqslant 5.7(1)$ T. Broad paramagnetic crystalline-electric-field excitations are observed. The spin-wave dispersion in the magnetically ordered phase exhibits a molecular-field splitting of 1.06(2) meV and an energy gap of 0.34(2) meV.

1. Introduction

Cerium in the rocksalt-type monochalcogenide CeSe carries a single localized 4f electron. The delocalized second excess valence electron fills part of a d band. It is responsible for the metallic properties of CeSe and influences the magnetic properties by modifying the exchange interactions [1]. The lowest-lying J-multiplet $^2F_{5/2}$ of the magnetic Ce^{3+} ion is split by the octahedral crystalline electric field (CEF) into a ground-state doublet Γ_7 and an excited-state quartet Γ_8. CeSe undergoes a second-order magnetic phase transition to a FCC antiferromagnetic type II structure [2] with the ordered moments μ parallel to the propagation vector $k = [\frac{1}{2}, \frac{1}{2}, \frac{1}{2}]$. The magnetic saturation moment of $\mu_0 = 0.57(5)\ \mu_B$ was found to be considerably reduced below the value 0.71 μ_B expected from the crystal-field ground-state doublet Γ_7. Such moment reductions are typical in Kondo systems.

Evidence that CeSe represents a dense Kondo compound comes from the measurement of the temperature dependence of the electric resistivity [3]. The magnetic part of the electric resistivity contains two well defined regions which are both proportional to $\ln T$. The low-temperature maximum around 5 K correlates with the onset of magnetic ordering. The second maximum in the neighbourhood of 100 K was assigned to conduction electrons scattered from the excited Γ_8 crystal-field levels.

|| Present address: H H Wills Physics Laboratory, University of Bristol, Bristol, UK.

0953-8984/93/081119+14$07.50

In CeSe the specific heat anomaly [1] around the Néel temperature T_N contains a magnetic entropy close to the value $R \ln 2 = 5.76$ J mol^{-1} K^{-1} expected for the splitting of the Γ_7 ground-state doublet upon magnetic ordering. Measurement of the specific heat anomaly of different CeSe samples [1] yielded a wide range of T_N between 5.0 K and 5.6 K. The magnetic-ordering temperature strongly depends on chemical composition and crystal perfection. In CeSe a distinct magnetic-field-induced phase transition was observed [1] in the magnetization along the [1 1 1] direction and is absent along [1 0 0].

We used a large CeSe single crystal of 140 mm^3 volume and performed elastic, diffuse critical and inelastic neutron scattering experiments to study the magnetic phase transition and magnetic excitations of the cerium monochalcogenide CeSe. We investigated the magnetic-field-induced phase transition in CeSe by neutron measurements in external magnetic fields up to 6 T. In addition we measured magnetoresistance and magnetization of CeSe up to 10 T. The results presented in section 3 and discussed in section 4 contain the critical exponents β, γ and ν, the anisotropy of the inverse correlation lengths, the magnetic-field-induced phase transition, paramagnetic CEF excitations and the spin-wave dispersion in the magnetically ordered state.

2. Experimental details

By Guinier x-ray diffraction we determined for the CeSe single crystal a room-temperature lattice constant $a = 5.9920(9)$ Å which is in agreement with the value given in the literature [4]. Under pure helium atmosphere the crystal was clamped with a vertical [1 $\bar{1}$ 0] axis to an aluminium sample holder. Elastic magnetic and diffuse critical neutron scattering experiments were performed on the double-axis spectrometer P2AX at the Saphir reactor in Würenlingen, Switzerland, using a standard ^{4}He cryostat and a neutron wavelength $\lambda = 2.337$ Å. A pyrolitic graphite filter of 10 cm length was inserted in the monochromatic beam to eliminate higher-order contamination.

With use of a superconductor magnet reaching 5 T an external magnetic field was applied vertical to the scattering plane. The possibility of the double-axis spectrometer P2AX to tilt the detector around a horizontal axis allowed to study also the behaviour of the magnetic peaks out of the scattering plane. A neutron wavelength of $\lambda = 1.050$ Å was used in this experiment.

By inelastic neutron scattering we measured crystalline-electric-field (CEF) excitations in the paramagnetic state and the spin-wave dispersion in the magnetically ordered state of CeSe. CEF transitions were measured on the triple-axis spectrometer IN5 (at the Saphir reactor) operated in the neutron energy-loss configuration. The energy of the scattered neutrons was kept fixed at 14.96 meV, giving rise to an energy resolution at $\Delta E = 0$ of 1.2 meV. A pyrolitic graphite filter was inserted into the outgoing neutron beam to reduce higher-order contamination.

Spin-wave excitations were measured on the triple-axis spectrometers IN12 and IN14 at the cold neutron source at the ILL in Grenoble, France. Constant-Q scans were performed along the symmetry directions $[\xi,\xi,\xi]$, $[0,0,\xi]$, $[0.5,0.5,\xi]$ and $[\xi,\xi,1-\xi]$ with the incoming neutron energy kept fixed at 8.29 meV, 4.98 meV and 3.78 meV, which yields instrumental energy resolutions at $\Delta E = 0$ of 0.43 meV, 0.20 meV and 0.13 meV, respectively. The data were corrected by $k_F^3 \cot(\theta_A)$ for

the varying analyser transmission [5]. Higher-order contamination was eliminated by a cooled Be filter in the monochromatic beam. In the IN12 experiment we used a superconductor magnet reaching 6 T and performed measurements at zero field and at $H = 6$ T.

A smaller piece of the same CeSe crystal was used to measure transverse magnetoresistance $\Delta\rho/\rho_0$ and magnetization $M(H)$ at 1.7 K in magnetic fields up to 10 T at the Department of Physics of Tohoku University at Sendai, Japan.

3. Results

3.1. The magnetic phase transition

The magnetic Bragg peaks detected below T_N correspond to the reported [2] FCC antiferromagnetic type II structure. No intensity was observed at the magnetic peaks $(\frac{1}{2},\frac{1}{2},\frac{1}{2})$ and $(\frac{3}{2},\frac{3}{2},\frac{3}{2})$ which leads to the conclusion that the ordered moments μ are parallel to the propagation vector $k = [\frac{1}{2},\frac{1}{2},\frac{1}{2}]$. A comparison of the magnetic $(-\frac{1}{2},-\frac{1}{2},\frac{3}{2})$ and the nuclear $(1,1,1)$ intensities yields an ordered magnetic moment of $\mu_0 = 0.56(6)\ \mu_B$ at 1.6 K. The temperature dependence of the reduced sublattice magnetization based on the peak intensity of the strongest magnetic reflection $(-\frac{1}{2},-\frac{1}{2},\frac{3}{2})$ is shown in the upper part of figure 1. In the temperature range $10^{-2} < [1-(T/T_N)] < 10^{-1}$ we fitted the power law $\mu/\mu_0 = A[1-(T/T_N)]^\beta$ to the reduced sublattice magnetization and obtained the following results for Néel temperature T_N, critical exponent β and constant A:

$$T_N = 5.12(2)\ \text{K} \qquad \beta = 0.36(3) \qquad A = 1.43(7).$$

For temperatures close to T_N we observe diffuse critical neutron scattering (DCNS) intensity near the magnetic peaks $(-\frac{1}{2},-\frac{1}{2},\frac{3}{2})$ and $(-\frac{3}{2},-\frac{3}{2},\frac{1}{2})$ but not at the peaks $(\frac{1}{2},\frac{1}{2},\frac{1}{2})$ and $(\frac{3}{2},\frac{3}{2},\frac{3}{2})$. This means that according to the polarization factor in the neutron cross section

$$\frac{d\sigma}{d\omega} \sim F^2(Q)\sum_{\alpha,\beta}(\delta_{\alpha,\beta} - Q^\alpha Q^\beta/Q^2)kT\chi^{\alpha\beta}(q,\omega=0,T) \qquad (1)$$

at the magnetic zone centres the longitudinal spin fluctuations (parallel to the direction of the ordered magnetic moments) are much stronger than fluctuations of other spin components. The temperature dependence of the DCNS intensity is shown in the lower part of figure 1. The Néel temperature determined from the sublattice magnetization is in nice agreement with the intensity maximum of the diffuse critical scattering (figure 1) which shows that the magnetic transition temperature is well defined in the crystal.

Diffuse Lorentzian peaks were measured at $(-\frac{1}{2},-\frac{1}{2},\frac{3}{2})$ parallel and perpendicular to the spin direction, along $q_\parallel = (\xi,\xi,\xi)$ and $q_\perp = (\xi,\xi,-2\xi)$, respectively. Lorentzian peaks along $q_\parallel$ and $q_\perp$ compared in figure 2 at three different temperatures show that for CeSe the observed DCNS intensity distributions are anisotropic in q-space. The widths at half maximum of the Lorentzian peaks directly yield the inverse correlation lengths $\kappa_\parallel$ and $\kappa_\perp$. We observe an almost temperature independent anisotropy of the correlation length of $\kappa_\parallel/\kappa_\perp = 0.79(10)$, which proves the

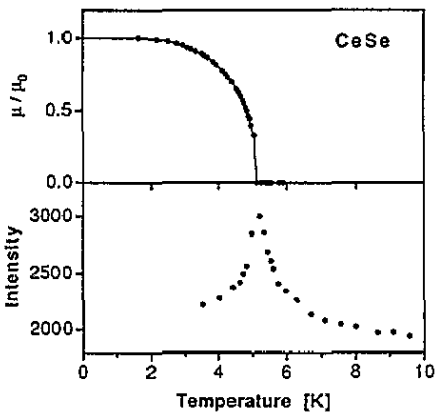

Figure 1. Upper part: temperature dependence of reduced sublattice magnetization of CeSe, based on the magnetic peak intensity of the reflection $(-\frac{1}{2},-\frac{1}{2},\frac{3}{2})$. Lower part: temperature dependence of diffuse critical scattering measured at $(-0.528,-0.528,1.556)$.

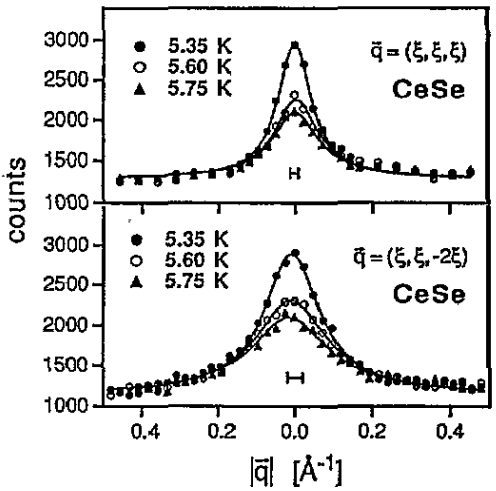

Figure 2. DCNS intensity distribution in CeSe at three different temperatures: q-scans through $(-\frac{1}{2},-\frac{1}{2},\frac{3}{2})$ parallel and perpendicular to the [1, 1, 1] direction show Lorentzian peaks with anisotropic widths. The solid lines are Lorentzian fits to the DCNS intensity. The experimental resolution is indicated by horizontal bars.

presence of anisotropic bilinear exchange interactions in CeSe. The critical exponents γ and ν were determined by fitting power laws to the susceptibility χ_0 and to the correlation length ξ, respectively. Within experimental uncertainty the Lorentzian peaks measured along $q_\parallel$ and $q_\perp$ yield identical values for the critical exponents of $\gamma = 1.32(12)$, $\nu = 0.61(10)$.

3.2. The magnetic-field-induced phase transition

Transverse magnetoresistance $\Delta\rho/\rho_0$ and magnetization of CeSe measured at saturation at 1.7 K are shown in figures 3(*a*) and (*b*), respectively. The phase transition occurs in a critical field $H_{crit} = 5.7(1)$ T along the [1 1 0] and [1 1 1] directions and is absent in magnetic fields along [1 0 0]. For $H < H_{crit}$ magnetoresistance and magnetization of CeSe both behave almost isotropically. At H_{crit} the big step-like decrease of 12% in the magnetoresistance along [1 1 0] and the steps of 0.03 μ_B in the magnetization along [1 1 0] and [1 1 1] determine the phase transition to be of first-order.

In an external magnetic field along the $[1\bar{1}0]$ direction we performed zero-field cooled neutron experiments at 1.6 K on IN12 spectrometer and at 4.2 K on P2AX spectrometer. At 1.6 K at saturation H_{crit} corresponds to 5.7(1) T. At $T = 4.2$ K the ordered moments have 75% of the saturation value (see figure 1) and H_{crit} is reduced to 4.1(1) T. In a FCC type II antiferromagnetic structure with the ordered moments μ parallel to the propagation vector $k = [\frac{1}{2},\frac{1}{2},\frac{1}{2}]$ the four non-parallel vectors $k_1 = [\frac{1}{2},\frac{1}{2},\frac{1}{2}]$, $k_2 = [-\frac{1}{2},-\frac{1}{2},\frac{1}{2}]$, $k_3 = [-\frac{1}{2},\frac{1}{2},\frac{1}{2}]$ and $k_4 = [\frac{1}{2},-\frac{1}{2},\frac{1}{2}]$ are equivalent.

For $H < H_{crit}$ the antiferromagnetic peaks of CeSe correspond to an antiferromagnetic type II structure with $\mu \| k$ and intensity is observed at magnetic

peaks corresponding to all four propagation vectors k_1, k_2, k_3 and k_4. For $H > H_{crit}$ the antiferromagnetic peaks of CeSe correspond also to an antiferromagnetic type II structure with $\mu \| k$ but intensity is observed only at magnetic peaks corresponding to the two propagation vectors k_1 and k_2 which are perpendicular to the direction of the magnetic field. The intensity of the antiferromagnetic peaks corresponding to the propagation vectors k_3 and k_4 disappears in the first-order phase transition at H_{crit}. When decreasing the magnetic field from $H > H_{crit}$ down to $H < H_{crit}$ the phase transition is fully reversible and the intensity of the antiferromagnetic peaks corresponding to k_3 and k_4 reappears. The hysteresis of H_{crit} is smaller than the experimental uncertainty of H_{crit} and could not be observed.

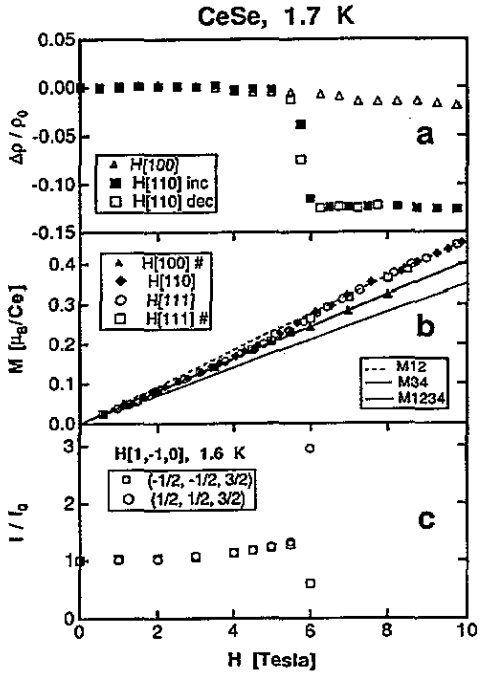

Figure 3. Magnetoresistance (*a*), magnetization (*b*) and field-dependent magnetic neutron intensities (*c*) of CeSe at saturation. #: data from [1].

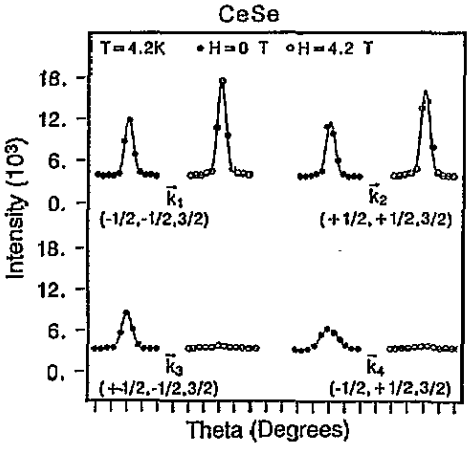

Figure 4. Neutron intensities of magnetic peaks corresponding to the four different propagation vectors k_1, k_2, k_3 and k_4 measured at 4.2 K below and above $H_{crit} = 4.1(1)$ T

Figure 4 shows intensities of magnetic peaks corresponding to the four different propagation vectors k_1, k_2, k_3 and k_4 measured at 4.2 K below and above H_{crit}. The field-dependent intensities of magnetic peaks corresponding to k_1 and k_2 measured at $T = 1.6$ K are plotted in figure 3(*c*). Magnetic peaks corresponding to k_3 and k_4 which are all out of the scattering plane could not be measured in the experiment on IN12 spectrometer.

With increasing magnetic field the canting of the magnetic moments due to the ferromagnetic alignment along the direction of the external magnetic field increases and leads to a reduction of the zero-field antiferromagnetic ordered moment. By using unpolarized neutrons we could not accurately determine the small induced ferromagnetic moment. However, a magnetic-field-induced reorientation of the

ordered antiferromagnetic Ce moments can be excluded since the magnetic peaks equivalent to $(\frac{1}{2},\frac{1}{2},\frac{1}{2})$ always have zero intensity at any measured magnetic field. Increasing the field $H[1\bar{1}0]$ from 0 T to 6 T we observe at 1.6 K a decrease of 10% in the sum of the magnetic elastic peak intensities (figure 3(*c*)) which gives rise to a reduction of the ordered antiferromagnetic moment from 0.56 μ_B at zero field to 0.53 μ_B at 6 T. On the other hand the magnetization (figure 3(*b*)) gives rise to an increase of the field induced ferromagnetic moment from 0 μ_B at zero field to 0.26 μ_B at $H[1\bar{1}0] = 6$ T. For $H > H_{crit}$ the field-induced ferromagnetic ordered moment is given by the line M12 in figure 3(*b*). For $H < H_{crit}$ the observed magnetization follows the line M1234 in figure 3(*b*) which is the average of the lines M12 (contributions from the vectors k_1 and k_2) and M34 (contributions from the vectors k_3 and k_4).

We summarize that at H_{crit} we observe a field-induced first-order magnetic phase transition from a canted FCC type II antiferromagnetic structure (at $0 < H < H_{crit}$) with contributions from k_1, k_2, k_3 and k_4 to a canted FCC type II antiferromagnetic structure with contributions from k_1, k_2. The average field-induced ferromagnet component increases with increasing external magnetic field and is given by the lines M1234 for $H < H_{crit}$ and M12 for $H > H_{crit}$ in figure 3(*b*).

3.3. Magnetic excitations

In the paramagnetic state of CeSe we observe broad CEF $\Gamma_7 \rightarrow \Gamma_8$ excitations. Spectra measured at 8 K at the nuclear Γ points (1, 1, 1) and (2, 2, 2) are shown in figure 5. The excitation at 10 meV (corresponding to 116 K) has a width at half maximum of 4.8 meV much bigger than the instrumental energy resolution. Along the cubic main symmetry directions $[00\xi]$, $[\xi\,\xi\,0]$ and $[\xi\,\xi\,\xi]$ the CEF $\Gamma_7 \rightarrow \Gamma_8$ transition exhibits a slight dispersion of about 1.5 meV with a roughly constant width and the minimum at the L point.

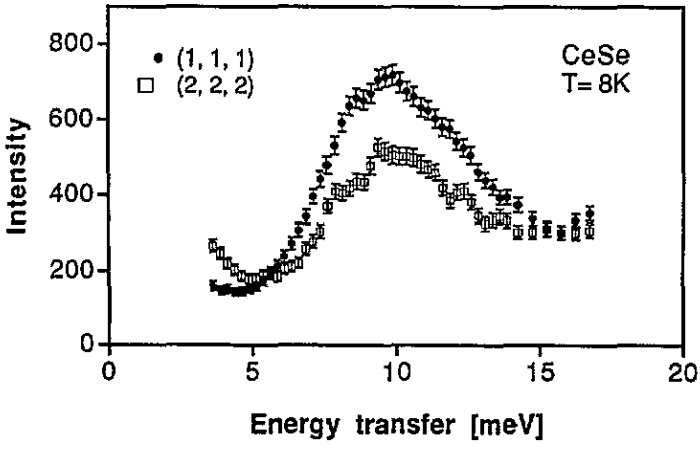

Figure 5. INS spectra of paramagnetic CeSe at 8 K, illustrating the CEF transition $\Gamma_7 \rightarrow \Gamma_8$ at the nuclear Γ point. The spectra were measured with constant analyser energy $E_A = 14.96$ meV.

In the magnetically ordered state the CEF ground-state doublet Γ_7 is split by the molecular field into two singlets. Spin-wave excitations of CeSe were measured at 1.6 K. We always refer to the full nuclear FCC Brillouin zone. Figure 6 shows the zero-field spin-wave dispersion along the high-symmetry directions $[\xi\,\xi\,\xi]$ and $[00\xi]$. We observe two excitation branches along $[\xi\,\xi\,\xi]$ and one branch along $[00\xi]$. The

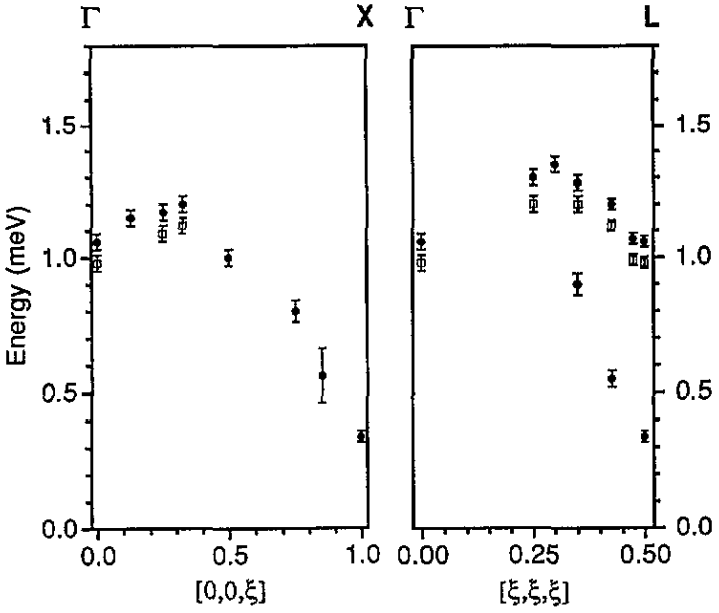

Figure 6. Observed spin-wave dispersion of CeSe at saturation along the high symmetry directions $[00\xi]$ and $[\xi\,\xi\,\xi]$ of the nuclear FCC Brillouin zone. Full and open symbols correspond to measurements at zero field and at $H[1\,\bar{1}\,0] = 6$ T, respectively. Excitation energies were determined by Gaussian fits. The energy of the transition shown at the X point was determined in the measurement at the L point.

spectra measured along the lower-symmetry directions $[\frac{1}{2}\,\frac{1}{2}\,\xi]$ and $[\xi\,\xi\,1-\xi]$ contain more than two excitations.

Figure 7 shows the excitation spectra measured at the L point $(\frac{1}{2},\frac{1}{2},\frac{1}{2})$ with the incoming neutrons fixed at three different energies. The spectra of figures 7(*a*) and (*b*) show a strong excitation at 1.06(2) meV with a width at half maximum of 0.44(6) meV which is about twice the instrumental energy resolution of figure 7(*b*). In addition, a weaker excitation is partly resolved at 0.35(6) meV in figure 7(*b*) and fully resolved at 0.34(2) meV in figure 7(*c*). The observed width of the lower energy excitation is 0.24(7) meV in figure 7(*b*) and 0.16(5) meV in figure 7(*c*) which basically corresponds to the instrumental energy resolutions of 0.20 meV and 0.13 meV in figures 7(*b*) and (*c*), respectively. From figure 7(*b*) we determine an intensity ratio of the two excitations of $I(\omega = 0.35\ \text{mev})/I(\omega = 1.06\ \text{meV}) = 0.17(8)$.

The two excitations shown in figure 7 correspond to dispersion minima and local intensity maxima. Along the $[\xi\,\xi\,\xi]$ direction the higher energy branch has a weak dispersion of about 0.3 meV (see figure 6). With distance from the L point the intensities of the excitations gradually decrease from 100% at the L point $(\frac{1}{2},\frac{1}{2},\frac{1}{2})$ down to 32% at the Γ point $(1,1,1)$. The lower-energy branch exhibits a strong dispersion near the L point. Compared to the weak intensity at $(\frac{1}{2},\frac{1}{2},\frac{1}{2})$ the energy-gap excitation is stronger at $(-\frac{1}{2},-\frac{1}{2},\frac{3}{2})$. However, due to the presence of the strongest magnetic Bragg peak at $(-\frac{1}{2},-\frac{1}{2},\frac{3}{2})$ this excitation could not be resolved there. In the branch along the $[00\xi]$ direction the intensities of the excitations become weak towards the X point. Due to the weakness of the excitation and the necessary high energy resolution the energy-gap excitation of 0.34(2) meV could not be resolved at the X points $(0,0,1)$ and $(1,1,0)$. But the dispersion along the $[00\xi]$ direction shown in figure 6 leaves no doubt that the 0.34(2) meV excitation is present at the X points. Except near the L points spin-wave measurements were performed with the energy of the incoming neutrons fixed at 8.29 meV (like in figure 7(*a*)). The resulting instrumental energy resolution did not allow a more detailed investigation of the widths of the spin-wave excitations in CeSe.

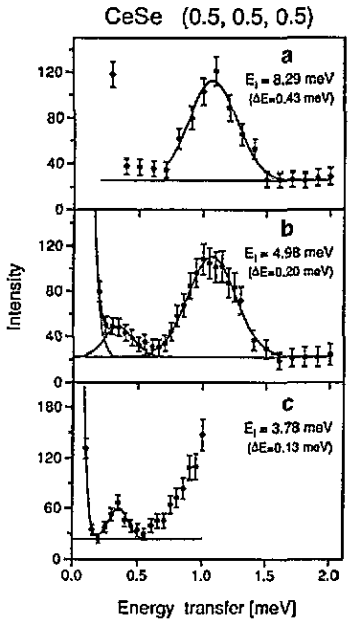

Figure 7. Observed excitation spectra of CeSe at the L point $(\frac{1}{2}, \frac{1}{2}, \frac{1}{2})$ measured at 1.6 K on spectrometer IN14 with E_I fixed at 8.29 meV (*a*), 4.98 meV (*b*) and 3.78 meV (*c*). Instrumental energy resolutions are given in parentheses. Solid lines are Gaussian fits to spin-wave excitations and to the elastic line.

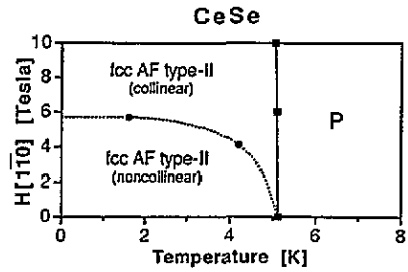

Figure 8. Suggested magnetic phase diagram of CeSe for magnetic fields along $[1\,\bar{1}\,0]$ as constructed from results of neutron diffraction (●) and specific heat (■, from [13]). P: paramagnet, AF: antiferromagnet. First- and second-order phase transitions are indicated by dashed and solid lines, respectively. Note that for $H > 0$ the antiferromagnetic structures are canted due to an additional field-induced ferromagnetic component along the $[1\,\bar{1}\,0]$ direction.

Due to the additional occurrence at the Γ point the higher-energy excitation at 1.06(2) meV in the spin-wave spectra at the L point can be identified to be the zone-centre excitation.

Spin-wave excitations measured above the magnetic-field-induced phase transition at $H[1\,\bar{1}\,0] = 6$ T are shown by open symbols in figure 6. The energy of the zone-centre excitation decreases from 1.06(2) meV at zero field to 0.98(2) meV at $H[1\,\bar{1}\,0] = 6$ T. The energy-gap excitation was not measured above the phase transition.

4. Discussion

4.1. The magnetic phase transition

The results determined for CeSe are summarized in table 1. The magnetic phase transition in CeSe is of second order and the critical exponents β, γ, ν agree within experimental uncertainty with the Heisenberg or Ising model [6]. In the series of the cerium monochalcogenides the same FCC antiferromagnetic type II structure [7,2] and within experimental error the same value for the critical exponent $\beta = 0.36$ [8,2] were determined for the compounds CeX (X = S, Se, Te).

Table 1. Magnetic properties of CeSe. $a_{295\,K}$: room temperature lattice constant; $\Gamma_7 \rightarrow \Gamma_8$: CEF splitting at the Γ point; k: magnetic propagation vector; ϑ_k^μ: angle between the direction of ordered magnetic moments and the magnetic propagation vector; μ_0: magnetic saturation moment; T_N: Néel temperature; β, γ, ν: critical exponents; $\kappa_\parallel/\kappa_\perp$: anisotropy of inverse correlation lengths; Δ_{MF}: molecular field splitting at saturation (spin-wave excitation at the Γ point); Δ_{gap}: spin-wave energy gap.

Nuclear structure	FCC
	$a_{295\,K} = 5.9920(9)$ Å
CEF level scheme:	$\Gamma_7 \rightarrow \Gamma_8$ (116 K)
Magnetic structure:	type II antiferromagnet
	$k = (\frac{1}{2}, \frac{1}{2}, \frac{1}{2})$
	$\vartheta_k^\mu = 0°$
	$\mu_0 = 0.56(6)\ \mu_B$
Phase transition:	second order
	$T_N = 5.12(2)$ K
	$\beta = 0.36(3)$
	$\gamma = 1.32(12)$
	$\nu = 0.61(10)$
	$\kappa_\parallel/\kappa_\perp = 0.79(10)$
Spin waves:	$\Delta_{MF} = 1.06(2)$ meV
	$\Delta_{gap} = 0.34(2)$ meV

The significantly anisotropic lenslike DCNS intensity distribution ($\kappa_\parallel/\kappa_\perp < 1$) in CeSe is similar to CeAs [9], whereas a cigarlike DCNS intensity distribution ($\kappa_\parallel/\kappa_\perp > 1$) was found in the compounds CeSb, CeBi, UN, UAs and USb [9]. For cerium and uranium monopnictides the correlation between the anisotropy $\kappa_\parallel/\kappa_\perp$ and the ordering temperature T_N, which is a measure of the strength of the exchange coupling, was empirically found [9] to be logarithmic in T_N:

$$\kappa_\parallel/\kappa_\perp = \text{constant} \ln T_N. \tag{2}$$

Equation (2) is also valid for the cerium monochalcogenides CeS [8] and CeSe [this work]:

CeS: $T_N = 8.48(2)$ K $\quad \kappa_\parallel/\kappa_\perp = 0.95(12)$

CeSe: $T_N = 5.12(2)$ K $\quad \kappa_\parallel/\kappa_\perp = 0.79(10)$.

Theoretical evidence for equation (2) is given in [10].

4.2. The magnetic-field-induced phase transition

When we proceed to discuss the magnetic structures of CeSe below and above the field-induced phase transition at H_{crit} we have to keep in mind that several spin arrangements are possible within the FCC type II antiferromagnetic structure with $\mu \| k$ observed in CeSe at zero field (see section 3.1). In the case of a collinear spin structure, magnetic order is described by only one propagation vector and the magnetic structure corresponds to a (+−) stacking of ferromagnetic planes along the direction of the propagation vector. In such a single-k structure at zero field four magnetic domains will develop, which correspond to the four equivalent propagation vectors k_1, k_2, k_3 and k_4 defined in section 3.2. When several k vectors exist the

magnetic order is non-collinear and dependent on the number of propagation vectors two-k, three-k and four-k structures are possible. At zero field the number of resulting magnetic domains is 6, 4 and 1 for a two-k, three-k and four-k structure, respectively. The main difference between these multi-k structures is the orientation of the magnetic moments which is plotted in figure 1 of [11].

Since in Fourier space there is no difference between separation or superposition, zero-field neutron diffraction experiments give identical patterns for collinear multidomain and non-collinear multidomain spin configurations. However, we can distinguish between the different spin arrangements by applying an external magnetic field, for example, parallel to the $[1\bar{1}0]$ direction and investigating the field-induced domain reorientation. In a collinear (single-k) spin structure the two domains characterized by k_1 and k_2 are favoured, since the magnetic moments are strictly perpendicular to the magnetic field and a two-domain state will be achieved. Similarly in a non-collinear two-k spin structure the domain defined by the pair of propagation vectors k_1 and k_2 is favoured with respect to the other five domains. For a complete domain reorientation only this domain must be observed with equal intensities for the k_1 and k_2 peaks.

Because in CeSe at $H > H_{crit}$ the observed antiferromagnetic peaks correspond to only two propagation vectors k_1 and k_2 the high-field magnetic structure of CeSe cannot be a three-k or four-k structure. Due to the pronounced asymmetry observed at 1.6 K and $H[1\bar{1}0] = 6$ T in the intensities of the k_1 and k_2 peaks (see figure 3(*c*)) also the possibility of a two-k structure can be eliminated. So we can unambiguously identify the magnetic structure of CeSe at $H > H_{crit}$ to be a canted collinear (single-k) structure.

To identify the spin configuration for $H < H_{crit}$ from the experimentally observed results of section 3.2 is more difficult. If we consider the possibility of the same canted collinear (single-k) spin arrangement at $H < H_{crit}$ we cannot explain the observed first-order phase transition at H_{crit}. In such a case the field-induced domain reorientation (which does not correspond to a magnetic phase transition) is expected to happen gradually with increasing field in contrast to experiment (figure 3(*c*)). And especially when decreasing the field from $H > H_{crit}$ the experimentally observed reappearance of the energetically unfavoured domains corresponding to k_3 and k_4 at the phase transition is incompatible with the possibility of a collinear spin configuration in CeSe at $H < H_{crit}$.

Our experiments therefore suggest the presence of a non-collinear spin configuration in CeSe at $H < H_{crit}$. Such an interpretation is supported by the results of dilatometric experiments [2], where a rhombohedral lattice distortion at $T < T_N$ expected for a single-k state could not be observed in CeSe by using Mo Kα x-ray radiation. CeSe remains cubic with an upper limit of 10^{-6} in contrast to, for example, TbP [12], where the first-order phase transition to FCC type II antiferromagnetic ordering with $\mu \| k$ is accompanied by a considerable rhombohedral lattice distortion.

The magnetic-field-induced first-order phase transition observed in CeSe then corresponds to a change from a canted non-collinear to a canted collinear spin configuration. Figure 8 shows the resulting tentative magnetic phase diagram of CeSe. We note that the observed magnetic-field dependent intensities (section 3.2) are in full agreement with the possibility of a canted four-k structure at $0 < H < H_{crit}$. But to definitively exclude the possibilities of a two-k or a three-k spin arrangement in CeSe at $H < H_{crit}$, further field-cooled experiments in magnetic fields along

lower-symmetry directions are necessary. The high-field behaviour of CeSe studied by free-powder magnetization experiments in a pulsed magnetic field up to 60 T is shown in [13]. The antiferromagnetic structure of CeSe is fully destroyed around 25 T where a kink in the magnetization curve indicates the saturation of the crystal-field ground-state doublet Γ_7.

UP [14] is an example for a first-order phase transition at zero field from a higher-temperature collinear single-k structure to a lower temperature non-collinear two-k structure.

4.3. Magnetic excitations

In CeSe hybridization between localized 4f electrons and conduction electrons (see maximum in the electric resistivity above 100 K, [3]) tends to delocalize the 4f states which gives rise to the observed broadening of the CEF $\Gamma_7 \rightarrow \Gamma_8$ transition. In addition this effect leads to the reduced value of the ordered magnetic saturation moment.

Some interest in the spin-wave dispersion of CeSe arises from the results of a similar study by Hälg and Furrer [15] on CeAs which undergoes a second-order phase transition to a FCC type I antiferromagnetic structure with $\mu \| k = [0, 0, 1]$ at low temperatures. The spin-wave dispersion of CeAs exhibits a transverse mode with a quadratic dispersion and a nearly zero energy gap at the X point. Due to the particular anisotropy of the magnetic exchange interactions CeAs represents an almost order-parameter-conserving antiferromagnet as theoretically explained by Prelovsek and Rice [16]. The spin-wave dispersion observed in CeAs was successfully analysed by a model [15] using a generalized Heisenberg Hamiltonian and the Green's function formalism in the random-phase approximation.

We used this model to perform an analysis of the observed zero-field spin-wave dispersion of CeSe. We assumed the presence of a multidomain single-k spin configuration in CeSe similar to CeAs. As a result the model fails to reproduce the observed spin-wave dispersion of CeSe which we illustrate in the following. The theoretical details as to how the model is adapted to the FCC antiferromagnetic type II structure with $\mu \| k$ are given in [17].

For isotropic bilinear magnetic exchange interactions $J(q)$ the calculated spin-wave excitation energies become

$$\omega(q) = \sqrt{(\Delta - MJ(q))(\Delta - MJ(q+k))}. \tag{3}$$

Δ is the molecular-field splitting and M denotes the matrix element. The magnetic-ordering vector k is different for each of the four magnetic domains. We consider nearest-neighbour coupling J_1 and next-nearest-neighbour coupling J_2. Due to the symmetry of nuclear and magnetic structure the multidomain spin-wave dispersion calculated from equation (3) consists of two excitation branches along $[\xi\,\xi\,\xi]$ and only one branch along $[00\,\xi]$ as observed experimentally (figure 6). The isotropic coupling parameters $J_1 = -0.089(6)$ meV, $J_2 = -0.045(3)$ meV and the molecular-field splitting $\Delta = 0.821(57)$ meV were obtained by first performing a least-square fit to the seven points of the higher-energy branch along $[\xi\,\xi\,\xi]$ (see figure 6) and then minimizing the energy of the calculated energy-gap excitation with the constraint that the values of J_1 and J_2 are inside the stability range of the antiferromagnetic type II structure (given by $J_2 < 0$ and $-2|J_2| \leqslant J_1 \leqslant |J_2|$). The resulting multidomain spin-wave dispersion is shown in figure 9. An isotropic calculation that describes

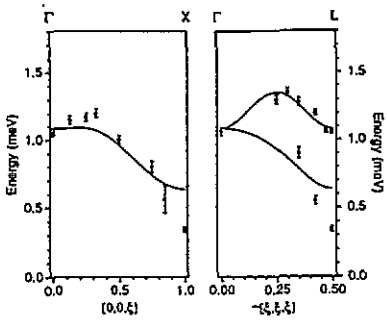

Figure 9. Calculated and observed spin-wave dispersion of CeSe. The solid lines correspond to a calculation for a single-k multidomain state with isotropic coupling parameters $J_1 = -0.089$ meV, $J_2 = -0.045$ meV and $\Delta = 0.821$ meV. Observed excitation energies are indicated by black points with error bars.

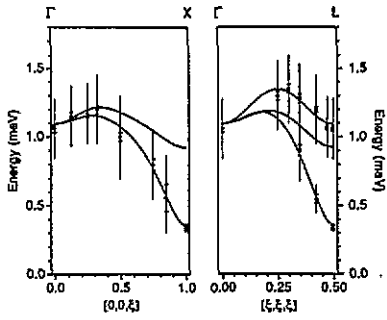

Figure 10. Calculated and observed spin-wave dispersion of CeSe. The solid lines correspond to a calculation for a single-k multidomain state with anisotropic coupling parameters $J^{l}_{1,d} = -0.091$ meV, $J^{t}_{1,d} = 0$ meV, $J_2 = -0.119$ meV and $\Delta = 1.078$ meV. Observed excitation energies are indicated by black points with error bars. The widths of the observed excitations are shown by vertical lines.

the rather flat higher-energy branch along $[\xi\,\xi\,\xi]$ fails to reproduce the observed low-energy excitations near the L and X points.

For anisotropic bilinear magnetic exchange interactions the scalar $J(q)$ becomes a tensor $J^{\alpha'\beta'}(q)$ (defined in [17]) and the spin-wave dispersion $\omega(q)$ splits into two different modes $\omega_1(q)$ and $\omega_2(q)$

$$\omega_1(q) = \sqrt{\Omega_1 - |\Omega_2|} \qquad \omega_2(q) = \sqrt{\Omega_1 + |\Omega_2|}$$

$$\Omega_1 = \Delta^2 - 0.5(A_0 + B_0 + A_1 + B_1)M\Delta + 0.5(A_0B_1 + B_0A_1 - 2C_0C_1)M^2$$

$$\begin{aligned}\Omega_2 = \{&\left[0.5(A_0 - B_0 - A_1 + B_1)M\Delta - 0.5(A_0B_1 - B_0A_1)M^2\right]^2 \\ &+ (C_0 - C_1)^2M^2\Delta^2 + (A_0C_1 + B_0C_1 - A_1C_0 - B_1C_0)(C_0 - C_1)M^3\Delta \\ &+ (A_0B_0C_1^2 - A_0B_1C_0C_1 - B_0A_1C_0C_1 + A_1B_1C_0^2)M^4\}^{1/2}\end{aligned}$$

$$A_0 = J^{x'x'}(q) \qquad B_0 = J^{y'y'}(q) \qquad C_0 = J^{x'y'}(q)$$

$$A_1 = J^{x'x'}(q+k) \qquad B_1 = J^{y'y'}(q+k) \qquad C_1 = J^{x'y'}(q+k). \tag{4}$$

which are degenerate only for q parallel to the magnetic propagation vector k. The resulting multidomain spin-wave dispersion consists of three excitation branches along $[\xi\,\xi\,\xi]$ and two branches along $[00\xi]$. A least-square fit of the lower-energy mode $\omega_1(q)$ of equation (4) to the observed excitations (18 points in figure 6) gives the result

$$J^{l}_{1,d} = -0.091(2) \text{ meV} \qquad J^{t}_{1,d} = 0.000(3) \text{ meV}$$
$$J_2 = -0.119(3) \text{ meV} \qquad \Delta = 1.078(24) \text{ meV}.$$

The strength of longitudinal nearest-neighbour coupling ($J^{l}_{1,d}$) for spin configuration parallel to the bond axis of the ions turns out to be much bigger than that of the transverse coupling $J^{t}_{1,d}$. Next-nearest-neighbour coupling (J_2) is isotropic. The observed excitations are well reproduced by the calculation as shown in figure 10. Along $[\xi\,\xi\,\xi]$ the calculated mode $\omega_2(q)$ that was not fitted lies fully inside the widths of the observed excitations of the higher-energy branch. Along $[00\,\xi]$ the calculated mode $\omega_2(q)$ disagrees with the experiment. The spectra measured in two different nuclear Brillouin zones at $(0, 0, \frac{3}{4})$ and at $(1, 1, \frac{1}{4})$ are shown in figure 11. The spectra contain an excitation at 0.80(4) meV and give no evidence for the presence of a second excitation as predicted by the model at 1.05 meV. However, the model gives an excellent description of the lenslike anisotropy of critical scattering ($\kappa_{\parallel}/\kappa_{\perp\mathrm{calc}} = 0.86$, $\kappa_{\parallel}/\kappa_{\perp\mathrm{obs}} = 0.79(10)$) and of the spin-wave intensities along the $[\xi\,\xi\,\xi]$ direction (e.g., for the two excitations shown in figure 7(*b*) the calculated intensity ratio of 0.20 agrees with the observed ratio of 0.17(8)). Furthermore the anisotropic bilinear exchange coupling $J^{\alpha'\beta'}(q)$ exhibits a maximum at $J^{z'z'}(k)$ at the magnetic ordering vector k which stabilizes the antiferromagnetic type II structure with $\mu \| k$.

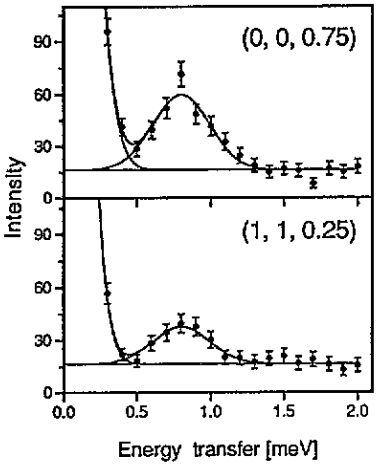

Figure 11. Observed excitation spectra of CeSe at $(0, 0, \frac{3}{4})$ and at $(1, 1, \frac{1}{4})$ measured at 1.6 K on spectrometer IN14 with E_I fixed at 8.29 meV. Solid lines are Gaussian fits to spin-wave excitations and to the elastic line.

Possible reasons for the failure of the spin-wave model are:

(i) The influence of Kondo hybridization which modifies magnetic exchange interactions cannot be neglected. But at present the appropriate form of the Hamiltonian including the effect of Kondo hybridization is not clear.

(ii) The model must be adapted to the correct spin configuration of CeSe. Since bilinear magnetic exchange interactions in CeSe are clearly anisotropic ($\kappa\|/\kappa_{\perp} \neq 1$!) the expressions for $\omega_1(q)$ and $\omega_2(q)$ calculated for a collinear spin configuration become more complicated than in equation (4) and we did not do such calculations.

Acknowledgments

We are indebted to Professor B R Cooper, Professor J Rossat-Mignod, Dr B Hälg and Dr W Bührer for stimulating discussions. Financial support by the Swiss National Science Foundation and by the Japanese Society for the Promotion of Science is gratefully acknowledged.

References

[1] Hulliger F, Natterer B and Ott H R 1978 *J. Magn. Magn. Mater.* **8** 87
[2] Ott H R, Kjems J K and Hulliger F 1979 *Phys. Rev. Lett.* **42** 1378
[3] Schoenes J and Hulliger F 1987 *J. Magn. Magn. Mater.* **63&64** 43
[4] Ott H R, Hulliger F and Stucki F 1978 *Inst. Phys. Conf. Ser.* **37** 72
[5] Dorner B 1972 *Acta Crystallogr.* A **28** 319
[6] Collins M F 1989 *Magnetic Critical Scattering* (Oxford: Oxford University Press)
[7] Schobinger-Papamanrellos P, Fischer P, Niggli A, Kaldis E and Hildebrandt V 1974 *J. Phys. C: Solid State Phys.* **7** 2023
[8] Dönni A, Furrer A, Fischer P and Hulliger F 1993 *Physica* B to be published
[9] Hälg B and Furrer A 1984 *J. Appl. Phys.* **55** 1860
[10] Kioussis N and Cooper B R 1986 *J. Magn. Magn. Mater.* **54–57** 701
[11] Herrmann-Ronzaud D, Burlet P and Rossat-Mignod J 1978 *J. Phys. C: Solid State Phys.* **11** 2123
[12] Bucher E, Maita J P, Hull G W, Longinotti L D, Lüthi E and Wang P S 1976 *Z. Phys.* B **25** 41
[13] Dönni A, Oyamada A, Ohe Y, Suzuki T, Sugiyama K, Date M, Fischer P, Furrer A and Hulliger F 1993 *J. Alloys Compounds* at press
[14] Burlet P, Quezel S, Rossat-Mignod J and Horyn R 1985 *Solid State Commun.* **55** 1057
[15] Hälg B and Furrer A 1986 *Phys. Rev.* B **34** 6258
[16] Prelovsek P and Rice T M 1987 *Phys. Rev. Lett.* **59** 1248
[17] Dönni A 1991 *Dissertation 9403* ETH Zürich